Vietnam Journal of Catalysis and Adsorption
Tạp chí xúc tác và hấp phụ Việt Nam

https://jca.edu.vn

Reactive Yellow 160 Degradation by a Peroxymonocarbonate-Based Advanced Oxidation Process: Performance and Mechanistic Insights

Vu Thi Tinh[1] , Vu Ngoc Duy[2], Nguyen Thi Bich Viet[1,*]

[1] *Faculty of Chemistry, Hanoi National University of Education, 136 Xuan Thuy road, Hanoi, VIETNAM*
[2] *Faculty of Chemistry, VNU University of Science, Vietnam National University, Hanoi, 19 Le Thanh Tong Str., Hanoi, VIETNAM*
** Email: vietntb@hnue.edu.vn*

ARTICLE INFO

Received: 15/08/2025
Accepted: 23/09/2025
Published: 30/09/2025

Keywords:
Reactive yellow 160;
advanced oxidation process (AOP);
peroxymonocarbonate (PMC);
reactive oxygen species (ROS);
radical scavengers

ABSTRACT

Peroxymonocarbonate (PMC)-based advanced oxidation systems have recently emerged as promising methods for treating textile wastewater. In this study, Reactive Yellow 160 (RY160) was selected as a target dye to investigate optimal operating conditions and elucidate the contributions of individual reactive oxygen species (ROS) in the PMC oxidation process. Experiments were performed under the optimized conditions of 0.061 mM RY160 (50 mg/L), 20 mM $NaHCO_3$, 50 mM H_2O_2, and 1.7 µM Co^{2+} at pH~9 (inherently buffered). Under these conditions, the RY160 degradation efficiency reached ~36% after 180 mins and increased to 99.7% with 30 min of UV irradiation. ROS quenching experiments indicated that hydroxyl radicals ($^{\bullet}OH$) and carbonate radicals ($CO_3^{\bullet-}$) were the primary oxidants, contributing 42% and 47%, respectively, to the overall degradation, while singlet oxygen ($^1O_2$) accounted for ~6%. The steady-state concentrations of $^{\bullet}OH$ and $CO_3^{\bullet-}$ in the PMC system were determined to be 7.64×10^{-13} M and 2.50×10^{-16} M, respectively. These findings provide mechanistic insight into PMC-mediated dye degradation and support its potential application in advanced wastewater treatment.

Introduction

The textile industry, in addition to consuming large volumes of water, generates substantial amounts of wastewater containing dyes and toxic, non-biodegradable organic compounds [1,2]. Dye-containing effluents can increase the turbidity of water bodies, elevate chemical oxygen demand (COD) and biological oxygen demand (BOD), thereby reducing dissolved oxygen levels and posing serious threats to aquatic ecosystems. Furthermore, these pollutants can enter the food chain, leading to drug resistance, bioaccumulation, and potential genotoxic or carcinogenic effects [3,4]. Among dyes, reactive dyes are widely used owing to their excellent color fastness, broad color range, and vibrant hues. However, these same properties make them highly resistant to degradation in wastewater environments [5–7]. Therefore, the development and application of effective, economical treatment methods for reactive dyes prior to discharge are imperative to mitigate the adverse impacts of the textile industry on ecosystems and human health.

Traditional treatment technologies, such as adsorption, membrane filtration, and biological processes, are commonly employed to remove pollutants from textile wastewater [6,8–12]. Physical methods, including adsorption and membrane filtration, can be effective for certain toxic organic compounds; however, they often suffer from incomplete removal, high operational

https://doi.org/10.62239/jca.2025.038

costs, and the need for frequent regeneration or replacement of saturated adsorbents or fouled membranes [8,10]. Biological methods employing microorganisms such as fungi or microalgae are environmentally friendly and cost-effective; however, they require long treatment times and exhibit markedly reduced efficiency at high dye concentrations or under sudden pH fluctuations [9,11,13]. In recent years, research on textile wastewater treatment has increasingly focused on advanced oxidation processes (AOPs), which rely on the generation of hydroxyl radicals ($^{\bullet}OH$) with high oxidative potential. Representative examples include the Fenton process, peroxone, H_2O_2/UV, O_3/UV, TiO_2/UV, and photocatalysis [6,14–16]. Among these, the Fenton and Fenton-like processes (using metal ions to activate H_2O_2) are widely studied for their effectiveness in decolorizing and decomposing toxic organic compounds. However, they are limited by a narrow optimal pH range (pH 2–4), low efficiency under neutral or weakly alkaline conditions, high chemical consumption to maintain acidic pH, and the generation of large amounts of sludge due to metal ion catalysts [17–19].

To overcome these drawbacks, PMC-based oxidation systems have emerged as a promising alternative, owing to their ability to operate efficiently under alkaline conditions and their potential to completely mineralize organic contaminants. PMC is generated in situ via the reaction between hydrogen peroxide (H_2O_2) and bicarbonate (HCO_3^-) or carbonate (CO_3^{2-}), producing multiple reactive oxygen species (ROS) such as peroxymonocarbonate (HCO_4^-), superoxide anion ($O_2^{\bullet-}$), singlet oxygen ($^1O_2$), carbonate radical ($CO_3^{\bullet-}$), hydroxyl radical ($^{\bullet}OH$), hydrocarbonate radical ($HCO_3^{\bullet}$), and hydroperoxyl radical ($HO_2^{\bullet}$) [14,20,21]. The presence of transition metal ions, particularly Co^{2+}, can markedly enhance the oxidative performance of PMC systems by catalyzing the decomposition of H_2O_2 and facilitating ROS generation through redox cycling between Co^{2+} and Co^{3+} [22–25]. Although the PMC/Co^{2+} system demonstrates high potential for textile wastewater treatment, its reaction mechanism, the optimal operating parameters for the degradation process of different dye types, and the quantitative contribution of individual ROS have not been fully elucidated.

Previously, the removal of Reactive Yellow 160 (RY160), a widely used reactive dye, has primarily relied on adsorption [26,27], photocatalysis [28,29], and AOPs [30–31]. Under typical conditions with an initial RY160 concentration of 50 mg/L, these methods achieved 70–90% removal within 120 minutes, depending on the treatment approach. For example, a Fenton process catalyzed by Fe(III)-modified laterite achieved 70% removal after 120 minutes under optimized conditions [31], whereas a nano ZrO_2-photocatalytic system reached 94% efficiency after 120 minutes of UV irradiation [28]. While these techniques demonstrated relatively high efficiencies, they still present notable limitations. Adsorption methods often generate secondary waste requiring further treatment, and Fe-based Fenton processes can lead to sludge accumulation, complicating downstream handling and disposal. Therefore, there is a strong need for alternative oxidation systems, such as PMC-based AOPs, which may offer high efficiency while minimizing secondary pollution.

In light of these gaps, the present study investigates the degradation of Reactive Yellow 160 (RY160) by a PMC-based system in the presence and absence of Co^{2+} catalyst. Key operational parameters, including catalyst dosage, oxidant concentration, and pH, were systematically optimized. Furthermore, the study identifies the contribution of distinct ROS to RY160 decolorization and quantifies the free radicals generated in the PMC system.

Experiments

Chemicals

Sodium bicarbonate, hydrogen peroxide, cobalt(II) nitrate, copper(II) nitrate, manganese(II) nitrate, nickel(II) nitrate, zinc(II) nitrate, iron(II) nitrate, dimethylamine (DMA), terephthalic acid (TA), sodium azide (NaN_3), *tert*-butanol (*t*-but), and ascorbic acid (AA) were purchased from Sigma-Aldrich. RY160 dye ($C_{15}H_{22}ClN_9Na_2O_{12}S_3$) was supplied by Xilong (China). All chemicals, except for the RY160 dye, were of analytical grade and used without further purification.

Methods

UV-Vis molecular absorption spectroscopy: The absorbance of RY160 solutions was measured at 427 nm using a Genesys 30 Visible Spectrophotometer (Thermo Scientific) after various reaction times. The decolorization efficiency of RY160 was calculated using equation (1): (Eq. 1), where C_0 and C_t are the initial RY160 concentration and the concentration at time *t*, respectively. The RY160 concentration was determined from the calibration curve: $A = (1.66 \pm 0.03) \times 10^{-5}\ C_{RY160} + (2.37 \pm 1.77) \times$

10^{-5} (μM) with a correlation coefficient R^2 = 0.9998, a limit of detection (LOD) of 2.04 × 10^{-3} mM, a limit of quantification (LOQ) of 6.80 × 10^{-3} mM, and a linear range from 1.22 × 10^{-3} mM to 0.122 mM at pH 9.0.

Molecular fluorescence spectroscopy: For DMA, fluorescence intensity was recorded at $\lambda_{em,\ DMA}$ = 360 nm (λ_{ex} = 298 nm); for hydroxylated TA (hTA), fluorescence was recorded at $\lambda_{em,\ hTA}$ = 425 nm (λ_{ex} = 315 nm) using an FL8500 Fluorescence Spectrophotometer (PerkinElmer).

Results and discussion

Factors influencing the decolorization of RY160

The effects of various parameters, including catalyst type, oxidant composition, oxidant concentration, pH, and UV irradiation, on RY160 decolorization were investigated at 25 °C with an initial dye concentration of 50 mg/L under the reaction conditions summarized in Table 1.

Table 1. Reaction conditions for the degradation of RY160 by the PMC system

Entry	pH	HCO_3^- (mM)	H_2O_2 (mM)	M^{2+} catalyst (μM)	UV
1	9	20	50	0	No
2÷6	9	20	50	0.1 ppm (Co^{2+}, Cu^{2+}, Ni^{2+}, Fe^{2+}, Mn^{2+})	No
7	9	0	50	0	No
8	9	0	50	1.7 (Co^{2+})	No
9÷13		5, 10, 30, 50, 70	12.5, 25, 75, 125, 175	1.7 (Co^{2+})	No
14÷18	6 - 11	20	50	1.7 (Co^{2+})	No
19	9	0	0	0	UV
20	9	0	25	0	UV
21	9	0	25	1.7 (Co^{2+})	UV
22	9	10	25	1.7 (Co^{2+})	UV

Catalyst effect and Co^{2+} activation mechanism

In Fig. 1(a), the results obtained from Entries 1÷6 reveal that the catalytic performance of the PMC system varied significantly depending on the transition metal ions present. While Ni^{2+} and Mn^{2+} reduced the decolorization efficiency and Fe^{2+} showed negligible influence, both Co^{2+} and Cu^{2+} enhanced the process. Notably, Co^{2+} exhibited the most pronounced improvement: after 180 min, RY160 removal in the PMC/Co^{2+} system was 2.9 times higher than in PMC/Cu^{2+} and 4.6 times higher than in PMC without a catalyst. Similar findings were also previously reported for the degradation of other reactive dyes by the PMC system [32-34]. The high catalytic activity of Co^{2+} can be rationalized by its electronic structure and redox flexibility. With a $3d^7$ configuration, Co^{2+} possesses three unfilled d orbitals that provide favorable orbital interactions with PMC, facilitating radical generation. Moreover, Co^{2+} readily undergoes redox cycling between Co^{2+} and Co^{3+}, enabling efficient electron transfer to sustain oxidative reactions. Although other tested metal ions (Fe^{2+}, Cu^{2+}, Ni^{2+}, Mn^{2+}) can also exist in multiple oxidation states and participate in electron exchange [35], their catalytic efficiency was considerably lower than that of Co^{2+}. In particular, the negative effects of Ni^{2+} and Mn^{2+} ions can be attributed to their tendency to catalyze H_2O_2 decomposition, which reduces the available PMC concentration in solutions and thus suppresses the degradation efficiency.

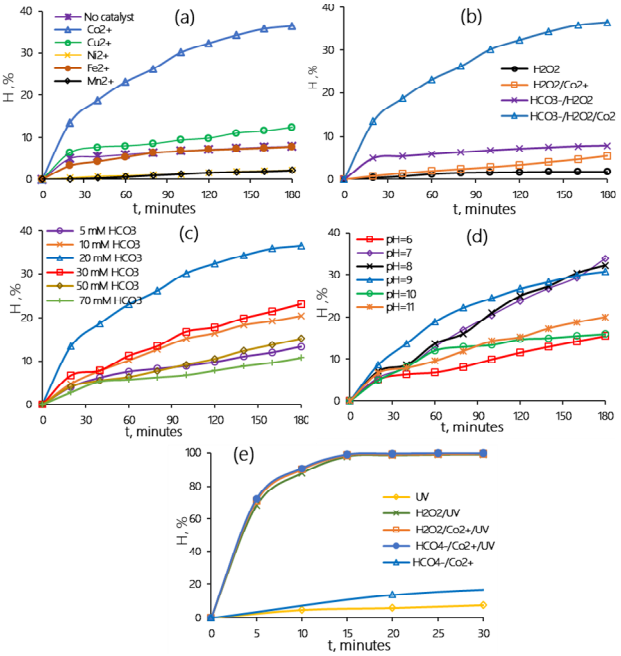

Fig 1. Influence of various factors on the decolorization efficiency of RY160: (a) catalysts, (b) oxidation system composition with and without Co^{2+}, (c) various HCO_3^- concentrations ((HCO_3^-: H_2O_2 molar ratio = 1: 2.5), (d) pH, and (e) UV irradiation in combination with different oxidation systems

The superior performance of Co^{2+} in PMC-based AOPs is specifically linked to its unique redox cycling ability with HCO_4^-. Co^{2+} readily coordinates with HCO_4^- to form an unstable complex that undergoes a one-

electron transfer, generating Co^{3+} along with ROSs such as $CO_3^{\bullet-}$ and $^{\bullet}OH$. Co^{3+} is then reduced back to Co^{2+} by H_2O_2 or other reductants, sustaining the catalytic cycle and continuous ROS generation [22-25], thereby accelerating RY160 degradation more effectively than other tested metals.

The main steps in the Co^{2+}/PMC redox cycle are:
PMC formation: $HCO_3^- + H_2O_2 \rightarrow HCO_4^- + H_2O$
PMC activation by Co^{2+}:
$HCO_4^- + Co^{2+} \rightarrow CO_3^{2-} + Co^{3+} + {}^{\bullet}OH$
$HCO_4^- + Co^{2+} \rightarrow Co^{3+} + OH^- + CO_3^{\bullet-}$
Co^{2+} regeneration:
$H_2O_2 + Co^{3+} \rightarrow HO_2^{\bullet} + Co^{2+} + H^+$
Radical transformation: $^{\bullet}OH + HCO_3^- \rightarrow CO_3^{\bullet-} + H_2O$

This Co^{2+}/Co^{3+} redox cycle enables continuous ROS generation without catalyst loss, accounting for the enhanced oxidation rate. The high selectivity of $CO_3^{\bullet-}$ toward electron-rich organic moieties complements the non-selective, high-potential oxidation by $^{\bullet}OH$, providing both efficiency and specificity in dye degradation.

Oxidation system composition

The effect of the oxidation system composition, studied with Entries 1, 2, 7, 8, and demonstrated in Fig. 1(b), highlights the synergistic effect between PMC and Co^{2+}. In the H_2O_2-only system, Co^{2+} slightly improved RY160 removal (1.76 % → 5.49 % in 180 mins) via slow Fenton-like $^{\bullet}OH$ generation under near-neutral medium (pH 9). In the PMC system, however, Co^{2+} boosted efficiency from 7.91% to 36.52%, owing to its ability to activate HCO_4^- through complex formation, as mentioned above, promoting decomposition into $^{\bullet}OH$ and $CO_3^{\bullet-}$ radicals. The latter provides selective oxidation while complementing the high reactivity of $^{\bullet}OH$. Even without Co^{2+}, the PMC/H_2O_2 system achieved 4.4-fold higher efficiency than H_2O_2 alone; with Co^{2+}, this rose to 6.7-fold higher than H_2O_2/Co^{2+}, reflecting dual activation of both HCO_4^- and H_2O_2. These trends align with prior studies on rhodamine B [32], reactive blue 19 (RB19) [33], and reactive blue 21 (RB21) [34], confirming PMC's superiority over conventional Fenton-like systems under near-neutral pH.

Oxidant concentration

The influence of oxidant concentration, represented by HCO_3^- (HCO_3^-: H_2O_2 molar ratio = 1:2.5), was investigated with Entries 2, 9÷13 and is shown in Fig. 1(c). Increasing HCO_3^- concentration from 5 mM to 20 mM improved decolorization efficiency due to enhanced HCO_4^- formation and ROS generation. The optimal efficiency occurred at the HCO_3^- concentration of 20 mM, while higher concentrations decreased performance as excess HCO_3^- and H_2O_2 promoted the reaction of H_2O_2 with $^{\bullet}OH$ to form less reactive hydroperoxyl radical ($HO_2^{\bullet}$), thereby lowering oxidation capacity. Consequently, 20 mM HCO_3^-: 50 mM H_2O_2 was selected as the optimal concentration for 50 mg/L RY160 treatment. Whereas the optimal concentration of HCO_3^-: H_2O_2 reported for 50 mg/L RB21 treatment was 50 mM: 100 mM [34].

pH effect

The effect of pH on RY160 decolorization, obtained from Entries 2, 14÷18, is illustrated in Fig. 1(d). Optimal efficiency was observed in near-neutral range (pH 7–9), consistent with the pH-dependent speciation of carbonate in the PMC system: HCO_3^- predominates near pH 8, CO_3^{2-} becomes dominant at higher pH, and CO_2 prevails under more acidic conditions. The predominance of HCO_3^- in this range not only favors HCO_4^- generation but also enhances its activation by Co^{2+}, which catalyzes the decomposition of HCO_4^- to yield ROSs such as $^{\bullet}OH$ and $CO_3^{\bullet-}$. This occurs through a redox cycle as mentioned above. Moreover, since the PMC system possesses inherent buffer capacity in the 8–9 range, no pH adjustment was required for effective RY160 treatment. Importantly, this pH range also supports efficient Co^{2+}/Co^{3+} cycling, ensuring sustained ROS production.

UV irradiation

The influence of pH on RY160 decolorization was studied with Entries 2, 19÷22. As shown in Fig. 1(e), UV irradiation markedly accelerated RY160 decolorization, with UV/PMC/Co^{2+}, UV/H_2O_2, and UV/H_2O_2/Co^{2+} systems all achieving >99% removal within 15 min. This enhancement arises from the photolysis of H_2O_2 and PMC under UV light, generating $^{\bullet}OH$ and $CO_3^{\bullet-}$ at a much higher rate. The rapid ROS generation under UV not only increases the oxidation potential but also synergizes with the Co^{2+}-mediated catalytic cycle, sustaining continuous radical production. In contrast, UV alone yielded only 7.54% removal after 30 min, confirming that photolysis without oxidants is insufficient. The PMC/Co^{2+} system without UV achieved ~15% removal, underscoring PMC's inherent oxidative capacity, but the dramatic rate increase with UV demonstrates the dominant role of photogenerated radicals in the overall process. These findings are consistent with previous reports on the UV/PMC and UV/H_2O_2 systems for other reactive dyes such as RB19 [33] and RB21 [34]. Notably, the performance here was better than that of the nano ZrO_2-photocatalytic

system reported by [28], which required 120 minutes of UV irradiation to achieve 94% removal of RY160.

Evaluation of ROS contribution to RY160 degradation

The role of individual ROS in RY160 degradation was assessed using selective scavengers: DMA for $CO_3^{\bullet-}$, *t*-but for $^{\bullet}OH$, NaN_3 for $^1O_2$, and AA for non-selective ROS quenching. All experiments were performed in a 100-mL reactor with magnetic stirring at 25 °C under the optimized conditions: 20 mM $NaHCO_3$, 50 mM H_2O_2, 1.7 µM Co^{2+}, pH ~ 9. Scavengers were added at varying concentrations: DMA (0.08, 0.16, and 0.21 mM) or *t*-but (0.5, 1, and 95 mM) or NaN_3 (10, and 15 mM) or AA (2.5, 5, and 10 mM), followed by an addition of 0.0611 mM RY160 dye. Dye degradation followed pseudo-first-order kinetics: $\ln\frac{C_t}{C_0} = -k \times t$ (Eq. 2) where k is the rate constant, C_0 and C_t are the initial and time-*t* concentration of RY160 dye. The relative contribution of each ROS was estimated using $\%\text{Contribution} = \frac{k_0 - k_q}{k_0} \times 100$ (Eq. 3), where k_0 and k_q are the rate constants without and with scavenger, respectively, which are determined from the linear kinetic plots of RY160 deradation over time as depicted in Figures 2 (b) – (e).

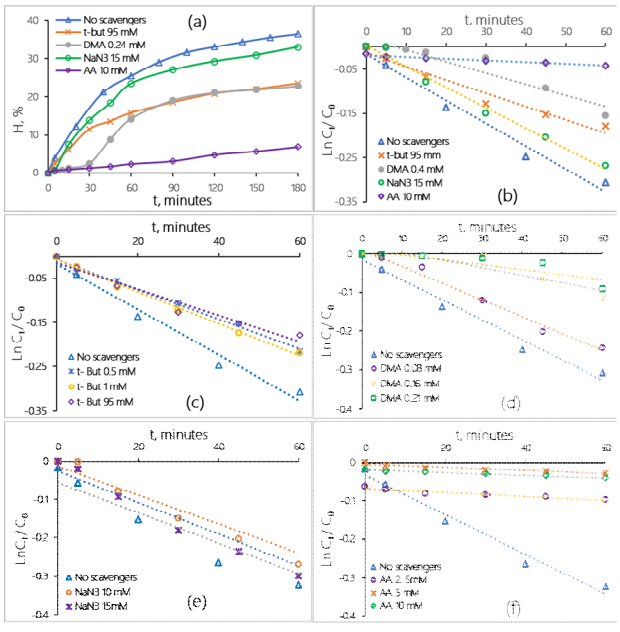

Fig 2: (a) Decolorization efficiency of RY160 over time and (b) Kinetic plots without and with various ROS scavengers: DMA, *t*-but, NaN_3, and AA. Kinetic plots of RY160 decolorization at different concentrations of individual scavengers: (c) *t*-but, (d) DMA, (e) NaN_3, and (f) AA.

As shown in Fig. 2(a), the addition of AA drastically reduced the removal efficiency to ~6% after 180 min, confirming that ROS-driven oxidation dominates the degradation pathway. A similar suppression trend was observed with *t*-but and DMA, indicating that $^{\bullet}OH$ and $CO_3^{\bullet-}$ are the two primary oxidants in the PMC system. In contrast, NaN_3 caused only a slight decrease in RY160 decolorization rate, suggesting a relatively minor role of $^1O_2$. Kinetic fitting of the first 60 min (Figs. 2b–e) yielded the contributions shown in Table 2: $^{\bullet}OH$ (47.0%), $CO_3^{\bullet-}$ (42.0%), $^1O_2$ (5.9%), and other oxidizing species (5.1%). These results demonstrate that $^{\bullet}OH$ and $CO_3^{\bullet-}$ contribute almost equally and account for ~90% of the total oxidative degradation of RY160 by the PMC system, whereas other ROSs contribute less than 10%.

Table 2. Contribution of individual ROS to RY160 degradation.

ROS	Scavengers	$k_q \times 10^3$, min^{-1}	Contribution (%)
$^{\bullet}OH$	TA	3.00	42
$CO_3^{\bullet-}$	DMA	2.74	47
$^1O_2$	NaN_3	4.84	5.9
all ROSs	AA	0.28	94.6
-	No scavenger	5.17	-

Interestingly, this contribution trend differs markedly from our previous work on reactive dye RB21 degradation using the PMC system (50 mM $NaHCO_3$, 100 mM H_2O_2, 1.7 µM Co^{2+} at pH ~ 9), where $CO_3^{\bullet-}$ accounted for 98.2% of the oxidation [34]. The shift in ROS contribution can be attributed to the differences in dye molecular structures. Structural features such as electron-withdrawing or electron-donating substituents, chromophore type, and steric hindrance can alter the reactivity toward $^{\bullet}OH$ or $CO_3^{\bullet-}$, favoring one pathway while diminishing the other. In the case of RY160, its structure appears to facilitate electrophilic attack by $^{\bullet}OH$, thereby increasing $^{\bullet}OH$'s relative role compared to $CO_3^{\bullet-}$.

Determination of the steady-state concentrations of $CO_3^{\bullet-}$ and $^{\bullet}OH$ radicals in the PMC system

Steady-state concentrations of $CO_3^{\bullet-}$ and $^{\bullet}OH$ radicals generated in the PMC system were estimated from their kinetic reactions with specific scavengers. Experiments were conducted in a 25-mL reaction vessel at 25°C with magnetic stirring. The PMC system consisted of 20 mM $NaHCO_3$, 50 mM H_2O_2, and 1.7 µM Co^{2+}, with either 0.2655 mM DMA ($CO_3^{\bullet-}$ scavenger) or 0.099 mM TA ($^{\bullet}OH$ scavenger). At certain time intervals *t* (minutes), 0.5-mL aliquots were taken and analyzed

for fluorescence emission to monitor radical quenching and calculate radical concentrations.

$CO_3^{\bullet-}$ radicals

DMA selectively reacts with $CO_3^{\bullet-}$ (k_1 = 1.8 × 10^9 M^{-1} s^{-1}) to form non-fluorescent products [36]. Since DMA itself fluoresces at 360 nm (λ_{ex} = 298 nm), its fluorescence decay can be directly correlated with $CO_3^{\bullet-}$ consumption. The kinetic relationship is given by: $\ln\frac{I_t}{I_0} = -k_1 \times C_{CO_3^{\bullet-}} \times t = -k_1' \times t$ (Eq-4) where I_0 and I_t are the initial and the time-*t* fluorescence intensities, respectively, and $k_1' = 1.8 \times 10^9 \times C_{CO_3^{\bullet-}}$.

From the fluorescence spectra of the reaction mixture over time (Fig 3a), the plot of $\ln(I_t/I_0)$ versus time *t* (Fig. 3b) yielded a slope of 0.0849 min^{-1}, giving a steady-state $CO_3^{\bullet-}$concentration of 7.64 × 10^{-13} M.

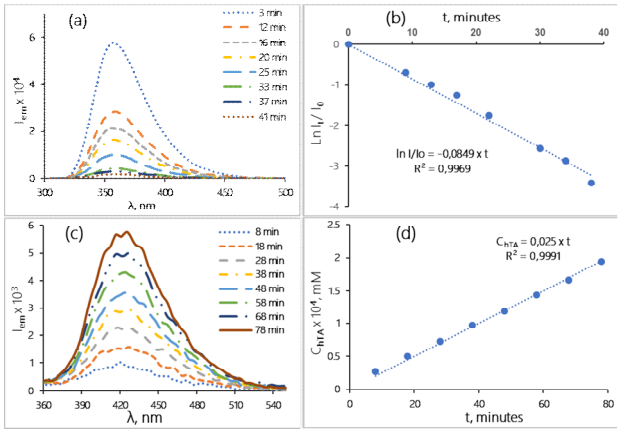

Fig 3. Fluorescence spectra of the reaction solution over time in the presence of (a) DMA for $CO_3^{\bullet-}$ detection and (c) TA for $^{\bullet}OH$ detection; Kinetic plots of the quenching reactions: (b) $CO_3^{\bullet-}$ quenching by DMA and (d) $^{\bullet}OH$ quenching by TA.

$^{\bullet}OH$ radicals

TA rapidly reacts with $^{\bullet}OH$ (k_2 = 4.1 × 10^9 M^{-1} s^{-1} [37]) to produce 2-hydroxyterephthalic acid (hTA), which fluoresces at 425 nm (λ_{ex} = 315 nm). The reaction follows second-order kinetics (Eq. 5):

$$r = \frac{d[hTA]}{dt} = k_2 \times [^{\bullet}OH] \times [TA] = k_2' \times [TA] \quad \text{(Eq. 5)}$$

where k_2 = 4,1. 10^9 $M^{-1}s^{-1}$, $k_2' = k_2 \times [^{\bullet}OH]$.

Under excess TA, pseudo-first-order behavior was assumed, leading to Eq. 6: $C_{hTA} = k_2'' \times t$ (Eq. 6), where $k_2'' = k_2 \times [^{\bullet}OH] \times [TA]$ is the slope obtained from the kinetic plot of hTA concentration (C_{hTA}) versus time *t* (Fig. 3d). This slope was 2.5 × 10^{-6} min^{-1}, corresponding to a steady-state $^{\bullet}OH$ concentration of 1.96 × 10^{-16} M, about three orders of magnitude lower than $CO_3^{\bullet-}$, which aligns with the prior findings [28].

This disparity in radical concentration, combined with the similar contributions of $^{\bullet}OH$ and $CO_3^{\bullet-}$ to overall degradation, explains the relatively low decolorization efficiency of RY160 by the PMC system in the absence of UV and the dramatic enhancement observed under UV irradiation.

Conclusion

The PMC system ($HCO_3^-/H_2O_2/Co^{2+}$) effectively degrades RY160 under slightly alkaline conditions, achieving ~40% decolorization after 180 mins without pH adjustment, and a complete removal within 30 mins under UV irradiation. ROS scavengers showed that $^{\bullet}OH$ and $CO_3^{\bullet-}$ are the main oxidants, contributing nearly equally to the degradation process, while $^1O_2$ and other ROS play only minor roles. The distinct ROS contribution pattern compared with RB21 degradation underscores the influence of dye molecular structure on oxidation pathways. Tailoring PMC operating conditions to target the dominant ROS pathway for specific dye structures can improve treatment efficiency, making this system a promising and adaptable approach for removing a broad spectrum of azo dyes from textile effluents, supporting its potential application in sustainable wastewater management.

References

1. B. Lellis, C.Z. Fávaro-Polonio, J.A. Pamphile, J.C. Polonio, Biotechnol. Res. Innov., 3 (2019) 275–290. https://doi.org/10.1016/j.biori.2019.09.001
2. W.L. Filho, P. Perry, H. Heim, M.A.P. Dinis, H.M. Moda, E. Ebhuoma, A. Paço, Front. Environ. Sci., 10 (2022). https://doi.org/10.3389/fenvs.2022.973102
3. S. Biyada, J. Urbonavičius, Clean. Eng. Technol., 24 (2025) 100905. https://doi.org/10.1016/j.clet.2025.100905
4. S. Biyada, M. Merzouki, Earthworm Technology in Organic Waste Management: Recent Trends and Advances, Elsevier, 2024, 339–357. https://doi.org/10.1016/B978-0-443-16050-9.00020-7
5. A. Soleimani-Gorgani, J. Color Sci. Technol., 6 (2012) 135–152. https://jcst.icrc.ac.ir/article_76047_en.html
6. J. Fadzli, K.H.K. Hamid, N.R.N. Him, S.W. Puasa, Desal. Water Treat., 257 (2022) 185–203. https://doi.org/10.5004/dwt.2022.28028
7. S.R. Maulik, A. Bhattacharya, P.P. Roy, K. Maiti, Textile Dyes and Pigments: A Green Chemistry Approach, Wiley Online, 2022, 17–44. https://doi.org/10.1002/9781119905332.ch2
8. M. Zeng, W. Wu, J. Fang, S. Li, Z. Zhou, J. Mater. Sci., 54 (2019) 9995–10008. https://doi.org/10.1007/s10853-019-03602-9

9. T.A. Aragaw, J. Hazard. Mater. Adv., 16 (2024) 100493. https://doi.org/10.1016/j.hazadv.2024.100493
10. G. Bayramoglu, G. Kunduzcu, M.Y. Arica, Polym. Eng. Sci., 60 (2020) 192–201. https://doi.org/10.1002/pen.25272
11. R. Khan, P. Bhawana, M.H. Fulekar, Rev. Environ. Sci. Biotechnol., 12 (2013) 75–97. https://doi.org/10.1007/s11157-012-9287-6
12. R. Al-Tohamy, S.S. Ali, F. Li, K.M. Okasha, Y.A.G. Mahmoud, T. Elsamahy, H. Jiao, Y. Fu, J. Sun, Ecotoxicol. Environ. Saf., 231 (2022) 113160. https://doi.org/10.1016/j.ecoenv.2021.113160
13. N.M. Marin, L.F. Pascu, A. Demba, M. Nita-Lazar, I.A. Badea, H.Y. Aboul-Enein, Int. J. Environ. Sci. Technol., 16 (2019) 6357–6366. https://doi.org/10.1007/s13762-018-2164-2
14. H. Pan, Y. Gao, N. Li, Y. Zhou, Q. Lin, J. Jiang, Chem. Eng. J., 408 (2020) 127332. https://doi.org/10.1016/j.cej.2020.127332
15. V. Katheresan, J. Kansedo, S.Y. Lau, J. Environ. Chem. Eng., 6 (2018) 4676–4697. https://doi.org/10.1016/j.jece.2018.06.060
16. L. Wang, L.J. Xu, Crit. Rev. Environ. Sci. Technol., 42 (2012) 251–325. https://doi.org/10.1080/10643389.2010.507698
17. B.T. Zhang, L. Kuang, Y. Teng, M. Fan, Y. Ma, J. Environ. Sci. (China), 105 (2021) 100–115. https://doi.org/10.1016/j.jes.2020.12.031
18. A. Babuponnusami, K. Muthukumar, J. Environ. Chem. Eng., 2 (2014) 557–572. https://doi.org/10.1016/j.jece.2013.10.011
19. F. Blanco, F. Torrades, M. De la Varga, J. García-Montaño, Desalination, 286 (2012) 394–399. https://doi.org/10.1016/j.desal.2011.11.055
20. N.A. Urbina-Suarez, C. Rivera-Caicedo, Á.D. González-Delgado, A.F. Barajas-Solano, F. Machuca-Martínez, Toxics, 11 (2023) 366. https://doi.org/10.3390/toxics11040366
21. K.Y. Mora-Bonilla, I.F. Macías-Quiroga, N.R. Sanabria-González, M.T. Dávila-Arias, ChemEngineering, 7 (2023) 86. https://doi.org/10.3390/chemengineering7050086
22. P. Hu, M. Long, Appl. Catal. B, 181 (2016) 103–117. https://doi.org/10.1016/j.apcatb.2015.07.024
23. X. Long, Z. Yang, H. Wang, M. Chen, K. Peng, Q. Zeng, A. Xu, Ind. Eng. Chem. Res., 51 (2012) 11998–12003. https://doi.org/10.1021/ie3013924
24. X. Li, Z. Xiong, X. Ruan, D. Xia, Q. Zeng, A. Xu, Appl. Catal. A Gen., 411–412 (2012) 24–30. https://doi.org/10.1016/j.apcata.2011.10.016
25. L. Zhou, W. Song, Z. Chen, G. Yin, Environ. Sci. Technol., 47 (2013) 3833–3839. https://doi.org/10.1021/es400101f
26. H.H.A. Ghafar, E.K. Radwan, N.M. Khalil, Y. Algamal, Egypt. J. Chem., 63 (2020) 2887–2899. https://doi.org/10.21608/ejchem.2020.21532.2291
27. F. Shariati, S. Shariati, M.A.A. Moghaddam, Desal. Water Treat., 212 (2021) 323–332. https://doi.org/10.5004/dwt.2021.26612
28. N. Al-Zaqri, A. Muthuvel, M. Jothibas, A. Alsalme, F.A. Alharthi, V. Mohana, Inorg. Chem. Commun., 127 (2021) 108507. https://doi.org/10.1016/j.inoche.2021.108507
29. J. Singh, V. Kumar, K.H. Kim, M. Rawat, Environ. Res., 177 (2019) 108569. https://doi.org/10.1016/j.envres.2019.108569
30. T.-A. Dang, T.V.A. Nguyen, Q.T. Do, S.D. Dao, Vietnam J. Chem., 56 (2018) 104–110. https://doi.org/10.15625/vjc.2018-0013
31. H.-D. Vu, T.T. Dang, T.-A. Dang, Sci. Tech. Dev. J.-Sci. Earth Environ., 3 (2019) 56–65. https://doi.org/10.32508/stdjsee.v3i2.465
32. T.H. Nguyen, T.H. Pham, H.T. Nguyen, B.N. Nguyen, N.D. Vu, T.B.V. Nguyen, Vietnam J. Chem., 60 (2022) 96–102. https://doi.org/10.1002/vjch.202200089
33. T.B.V. Nguyen, N. Nguyen-Bich, N.D. Vu, H. Ho Phuong, H. Nguyen Thi, J. Anal. Methods Chem., 2021 (2021) 6696600. https://doi.org/10.1155/2021/6696600
34. V.T. Tinh, N.T.B. Viet, HNUE J. Sci.: Nat. Sci., 69 (2024) 96–104. https://doi.org/10.18173/2354-1059.2024-0039
35. S. Gupta, R. Fernandes, R. Patel, M. Spreitzer, N. Patel, Appl. Catal. A Gen., 661 (2023) 119254. https://doi.org/10.1016/j.apcata.2023.119254
36. L. Wojnárovits, T. Tóth, E. Takács, Sci. Total Environ., 717 (2020) 137219. https://doi.org/10.1016/j.scitotenv.2020.137219
37. S.E. Page, W.A. Arnold, K. McNeill, J. Environ. Monit., 12 (2010) 1658–1665. https://doi.org/10.1039/C0EM00160K